

Size control of Pt nanoparticles with stabilizing agent for better utilization of the catalyst in fuel cell reaction

S. Singh · J. Datta

Received: 14 September 2009 / Accepted: 8 February 2010 / Published online: 6 March 2010
© Springer Science+Business Media, LLC 2010

Abstract In this investigation, tetrabutylammonium bromide (TBAB) has been used as the stabilizing agent during synthesis of 20% Pt on Vulcan XC-72 carbon support by the sodium borohydride reduction method. Crystallographic and morphological properties of the prepared electrocatalysts as well as their surface area were determined employing the respective techniques such as X-ray diffraction, transmission electron microscopy, and Brunauer–Emmet–Teller method. TBAB in the chemical deposition bath was found to control the size of nanoparticles by preventing the metal particles to aggregate during the reduction process without interfering with the deposition phenomenon. The catalysts were further characterized electrochemically by the help of cyclic voltammetry, steady state polarization, chronoamperometry, and impedance spectroscopy confirmed that the optimal use of tetrabutylammonium bromide produces fine grain Pt nanoparticles acting as the electrocatalyst for ethanol oxidation and can successfully prevent the use of excess of Pt that usually remain unutilized in the bulk of the catalyst.

Introduction

To date, the direct alcohol fuel cell (DAFC) is considered to be one of the promising electrochemical devices in view of its high energy-conversion efficiency, low pollutant emission, and advantages like easy fuel delivery and storage, no need for reforming and favorable power capability, compared with other fuel cell systems [1].

Carbon-supported Pt nanoparticles remain the choice for electrocatalysts of fuel cells, because of their electrocatalytic activities for both the oxidation of hydrogen and alcohol on the anode and the reduction of oxygen on the cathode. It is known that the catalytic activity depends on the particle size, shape, size distribution, and dispersion over the catalyst support [2–7]. Thus, preparative strategies of well-dispersed Pt nanoparticles with narrow size distribution play an important role in view of their better electrocatalytic activity for fuel cell reactions. Various methods have been employed to prepare carbon-supported Pt nanoparticles, for example electrochemical deposition [8–10], micro emulsion [11, 12], reduction of Pt precursor by reducing agents such as bisulfate, borohydride, hydrazine, formaldehyde and formic acid [13–18], and so on. However, with these conventional methods, it is difficult to achieve desired sizes of Pt nanoparticles within the range of 2–5 nm with homogeneous dispersion on the carbon support. Considering impregnation-reduction method by sodium borohydride (NaBH_4), the major drawback is the lack of size control of metal particles; specially reducing the particle size down to 5 nm is still a big challenge for this method. Hence, to tailor the size of Pt nanoparticles with uniform dispersion on the carbon support, some kind of stabilizing agents, such as surfactants, ligands or polymers, are usually employed during the preparative process [19–26]. Recently, the use of capping agents such as tetraalkylammonium salts (NR_4^+), triphenylphosphine (PPh_3), polyvinyl pyrrolidone (PVP), and polyvinyl alcohol (PVA) has attracted attention, because the narrow size distribution can be achieved through stabilization either by steric hindrance or by electrostatic charges during the synthesis [27].

In the present investigation, well-dispersed 20% C/Pt nanocatalysts have been prepared by the reduction of chloroplatinic acid (H_2PtCl_6) with NaBH_4 using tetrabu-

S. Singh · J. Datta (✉)
Department of Chemistry, Bengal Engineering and Science
University, Shibpur, Howrah 711103, West Bengal, India
e-mail: jayati_datta@rediffmail.com; susmitachem@yahoo.co.in

tylammonium bromide (TBAB) as the stabilizing agent for the study of electrochemical oxidation of ethanol. The TBAB used in the preparation of C/Pt nanocatalysts was thoroughly removed from the matrix of Pt particles, prior to subjecting the catalyst particle to any kind of investigation. The crystal phase, morphology, and surface area of the nanoparticles have been studied by X-ray diffraction (XRD), transmission electron microscopy (TEM), and Brunauer–Emmet–Teller (BET) method, respectively. Finally, the catalytic activity, toward ethanol oxidation, of the modified Pt electrodes prepared at different levels of TBAB has been thoroughly investigated by the electrochemical techniques such as cyclic voltammetry (CV), potentiostatic polarization, chronoamperometry, and electrochemical impedance spectroscopy (EIS).

Experimental

Preparation of catalysts

C/Pt nanocatalysts of 20 wt% were prepared through impregnation-reduction method from the chemical bath composed of 0.002-M H_2PtCl_6 (Arora Matthey Ltd.) and varying levels of TBAB (Sigma–Aldrich) corresponding to the Pt/TBAB molar ratios of 5:1, 3:1, 1:1, and 1:3. The respective Pt catalysts produced from the different bath solutions have been henceforth denoted as C/Pt-a, C/Pt-b, C/Pt-c, and C/Pt-d in this article. During synthesis, initially an appropriate amount of Vulcan XC-72 carbon (Cabot India) was added to the 400-mL milli-Q water ($\rho = 18.2 \text{ M}\Omega \text{ cm}$) and the mixture was ultrasonicated for 30 min. This was followed by sequential addition of the respective Pt-precursor and TBAB solutions to this mixture and was stirred for 1 h. Subsequently 0.05-M NaBH_4 (Merck) solution was added, drop by drop and in excess, to the mixture with vigorous stirring until the brown colloidal solution become colorless containing dispersed black Pt particles for the complete reduction of Pt from the precursor salt. The resulting heterogeneous colloidal mixtures were allowed to stir for 1 h at room temperature and centrifuged. Then, black Pt catalyst particles were isolated by centrifugation and the supernatant colorless liquid was tested by silver nitrate to detect the presence of any residual bromide ion in solution. The catalyst was washed with plenty of milli-Q water and bromide test was done until supernatant liquid gave the negative test of it. The catalyst was dried in oven at 100 °C for 2 h. To ensure removal of the organic moieties of the TBAB remaining in the C/Pt catalysts, prior to the morphological and electrochemical measurements, the catalysts powders were dispersed in ethanol and ultrasonicated for 15 min. Then, they were centrifuged in excess ethanol at the speed of 5,000 rpm for 15 min and the treated ethanol was

siphoned off. This centrifugation process was repeated five times. Finally, the catalysts were dried in an oven at 50 °C for 1 h to remove the trace amount of alcohol.

Surface characterization and morphological studies

To determine the crystalline nature of the catalyst particles, X-ray diffractograms were obtained by a SEIFERT 2000 diffractometer operating with CuK_α radiation ($\lambda = 0.1540 \text{ nm}$) generated at 35 kV and 30 mA. Scans were recorded at 1 min^{-1} for 2θ values between 2° and 90°. The (111) peak of the Pt face centered cubic (f.c.c.) structure was selected for estimating the volume weighted average crystallite size from XRD, using Scherrer equation. The recorded XRD patterns were analyzed following the Joint Committee on Powder Diffraction Standard (JCPDS) file. To get the morphology and the volume weighted average particle size, TEM images of Pt catalysts were obtained using FEI model STWIN operated at an accelerating voltage of 200 kV. Specimens for TEM analysis were prepared by ultrasonically suspending the particles in alcohol in an ultrasonic cleaner (Model AU-30C, 4-L capacity, 100 W, 28 kHz, 130 VA, timer 15 min, Eyela, Tokyo, Rikakikai Co., Ltd). A drop of the suspension was deposited onto a standard carbon-coated Cu grid and allowed to dry before being inserted into the microscope. The particle size distribution histograms obtained by the observation of about 250 particles from the four different locations of the corresponding TEM images. The real surface area of each of the catalysts was determined at 77 K by the BET method using nitrogen as the adsorbate in Quantachrome Autosorb instrument (Model AS1-CT). Prior to the measurements, samples were out gassed at 300 °C for 1 h to remove residual water and gases. The surface area according to BET theory has been evaluated using the multipoint method at relative pressure up to $P/P_0 = 0.2$ and the total volume (V_{tot}) was calculated from the volume of nitrogen adsorbed at near to saturation pressure, $P/P_0 = 0.99$. The volume of micropores (V_{m}) was derived from the so-called t plot dependence of nitrogen sorption isotherm. The pore size distribution was derived from adsorption isotherm according to Barrett–Joyner–Halenda (BJH) model calculations.

Preparation of electrodes

Saw cut finish grade graphite plate (GLM grade, Graphite India Ltd) of thickness approximately 2 mm was used as support for the working electrode. A catalyst ink was prepared by taking appropriate amount of catalyst in 5 wt% Nafion ionomer (Electrochem. Inc, USA) and 2-propanol (GR grade, Merck) and the mixture was sonicated. A calculated amount of this slurry was micropipetted out onto the graphite support (0.65 cm^2) to maintain a constant

catalyst loading of 0.50 mg cm^{-2} . Notably, a major part of the investigations involved the study of electrocatalytic activity and loading of Pt is kept low used in each of the TBAB-stabilized carbon-supported catalyst (C/Pt). However, such investigations were also extended to higher loading of the non-protected C/Pt catalysts (0.77 and 1.2 mg cm^{-2}) for comparison.

Electrochemical measurements

Electrochemical measurements were conducted using a computer-controlled potentiostat/galvanostat with PG STAT 12 and FRA modules (Ecochimie B.V., The Netherlands). Experiments were carried out in a glass cell using conventional three-electrode set-up incorporating mercury/mercurous sulfate (MSE) reference electrode and a bright Pt-foil ($10 \text{ mm} \times 10 \text{ mm}$) counter electrode at room temperature. The geometrical area of the electrocatalyst exposed to the solution was always 0.65 cm^2 . All the potentials in this article are referenced to the standard hydrogen electrode (SHE) at cell operating temperature and the current is normalized to the geometrical surface area. All test solutions were prepared using milli-Q water. During conducting each electrochemical measurements, the surface of the working electrode was cleaned electrochemically prior to the addition of 1-M ethanol (AR grade, Merck) to the electrolyte, by cycling the potential between -0.8 and 0.9 V at 50 mV s^{-1} in 0.5-M sulfuric acid (AR grade, Merck) until there was no change in the voltammetric feature. All the solutions were purged with nitrogen gas (XL grade, BOC India Ltd.) for 30 min before starting each of the electrochemical experiment. Cyclic voltammograms were obtained for 1-M ethanol (EtOH) electro-oxidation at a sweep rate of 50 mV s^{-1} within the potential range -0.8 – 1.2 V . Steady state potentiostatic data were noted after polarization for 5 min and chronoamperograms were recorded for 1 h at the electrode potential of -0.1 V . Allowing equilibration for 30 s, electrochemical impedance measurements were performed at the desired potential of -0.1 V in the frequency range, from 30 kHz to 30 MHz, containing 80 data points.

Results and discussion

Figure 1 shows the XRD patterns of carbon-supported nonprotected 20% Pt catalyst and TBAB-stabilized Pt catalysts such as C/Pt-a, C/Pt-b, C/Pt-c, and C/Pt-d. The XRD patterns of Pt exhibited diffraction peaks of (111), (200), (220), (311), and (222) planes corresponding to an f.c.c. crystal structure (JCPDS 04-0802). The average crystallite size (D , nm) for the Pt nanocatalysts in each of

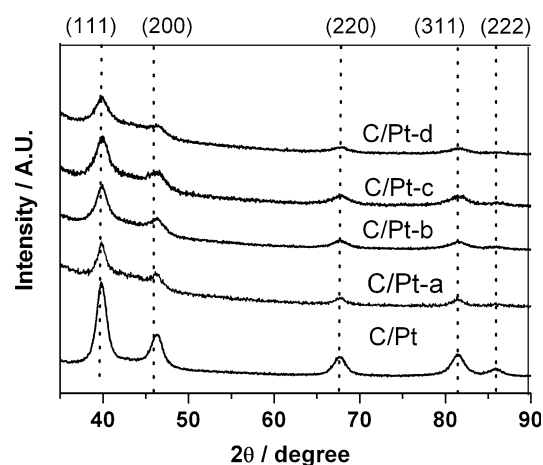


Fig. 1 XRD patterns of C/Pt and TBAB-stabilized C/Pt catalysts

the catalysts was calculated from broadening of the (111) diffraction peak using Scherrer equation:

$$D = \frac{0.9\lambda}{B \cos \theta} \quad (1)$$

where λ is the wavelength of the X-ray (1.54056 \AA), θ is the angle at the maximum of the peak, and B is the width of the peak at half height. Subsequently, the specific chemical surface area (S , $\text{m}^2 \text{ g}^{-1}$) for Pt particles was calculated from the following equation based on the assumption of spherical morphology [19]:

$$S = \frac{6000}{D\rho} \quad (2)$$

where D is the mean diameter of the particles (nm) as obtained from XRD studies in the present investigation and ρ is the density of Pt (21.4 g cm^{-3}).

Electrochemical active surface (EAS) areas of the different catalysts were derived from cyclic voltammometric studies. Figure 11 shows the cyclic voltammograms obtained in 1.0-M H_2SO_4 for C/Pt and the different protected C/Pt electrodes. EAS of catalysts was evaluated by means of following equation:

$$\text{EAS} = \frac{Q_H}{[\text{Pt}] \times 0.21} \quad (3)$$

where $[\text{Pt}]$ represents the platinum loading (mg cm^{-2}) in the electrode, Q_H the amount of charge exchanged during the electroadsorption of hydrogen atoms ($\text{Pt} + \text{H} + e^- \rightarrow \text{Pt-H}$) on Pt (mC cm^{-2}) and 0.21 (mC cm^{-2}) is associated with the charge required to oxidize a monolayer of H_2 on poly-crystalline Pt electrodes. Table 1 summarizes the EAS values of all the catalysts. Roughness factor, R_f , which describes the enhancement of the real electrochemical surface area in comparison with the geometric area, for each of the catalyst is determined from the linear relationship between R_f and Pt loading (W , mg cm^{-2})

Table 1 Comparison of morphological data of the carbon-supported 20% Pt and TBAB-stabilized Pt catalysts

Electrocatalysts	Particle size from TEM (nm)	Crystallite size from XRD (nm)	Specific chemical surface area ($\text{m}^2 \text{g}^{-1}$)	Electrochemical surface area ($\text{m}^2 \text{g}^{-1}$)	Roughness factor
C/Pt	4.5	4.9	57.2	47.5	286.0
C/Pt-a	5.5	3.4	82.5	73.2	412.5
C/Pt-b	3.5	2.8	100.1	92.4	500.5
C/Pt-c	2.5	2.5	112.1	110.0	560.0
C/Pt-d	–	1.5	186.9	170.5	934.5

$$R_f = SW \quad (4)$$

The morphological data for the prepared catalysts are presented in Table 1. There is a distinct fall in size with the increase in TBAB content in the preparative bath. As a consequence, the specific surface area and the roughness factor of the catalyst matrix increase.

Figures 2, 3, 4, 5, and 6 represent the high-resolution TEM images and the particle size distribution of all the nanocatalysts prepared. Figure 2a represents the nonprotected Pt particles accumulated as lumps on many parts of the carbon support. However, the catalyst matrix is found to be enriched with well-dispersed finer particles mostly of spherical shape as the amount of stabilizing agent is increased in the preparative bath (Figs. 3a, 4a, 5a). The clear trade-off in size matches with the order of discreteness of the particles in the catalysts from C/Pt-a to C/Pt-c. On the other hand, the HRTEM image of C/Pt-d shows a more snow-like appearance of the matrix on which the Pt nanoparticles remain embedded in Fig. 6a. This imparts an all together different textural character which is later discussed in the BET investigation. Figures 2b, 3b, 4b, and 5b show the size distribution plot of C/Pt, C/Pt-a, C/Pt-b, and C/Pt-c, respectively, and the size distribution is found to be narrower with almost 95% of the catalyst particles in the

2–3-nm range with pronounced dispersion on the carbon support in case of C/Pt-c catalyst. This also corroborates with an earlier report on particle size distribution against Pt loading [28]. This study [28] demonstrated that particle size is confined to ~ 2.5 nm only with a 20% catalyst loading. However in this study, the C/Pt-a and the C/Pt-b catalyst off using different levels of TBAB are characterized by their respective particle size of approximately 5–6 and 3–4 nm. All the catalysts reveal their polycrystalline nature in the selected area diffraction patterns (SADP) in Figs. 2c, 3c, 4c, 5c and 6b. The diffraction pattern shown in Fig. 2c indicates the formation of nanophases of the C/Pt as identified by the characteristic rings of f.c.c. crystal structure. Among all the SADP images, Figs. 4c and 5c for C/Pt-b and C/Pt-c show the absence of agglomeration as observed by the smooth crystalline rings which are indexed for f.c.c. crystal structure and Figs. 3c and 6b show good crystallinity of C/Pt-a and C/Pt-d catalysts, respectively, intermixed with some coarse particles. The fringe patterns for the C/Pt-c catalyst are shown in Fig. 7, where the crystalline plane of the spherical Pt is evident. The 0.2259-nm spacing which is attributed to the Pt (111) plane (JCPDS 04-0802) of the f.c.c. lattice is indicated by the arrow in Fig. 7. Compared to the nominal Pt (111) spacing of 0.226 nm (JCPDS 04-0802), the spacing was nearly

Fig. 2 a HRTEM image, b particle size distribution, and c selected area diffraction pattern (SADP) of C/Pt. The rings are indexed for an f.c.c. crystal structure

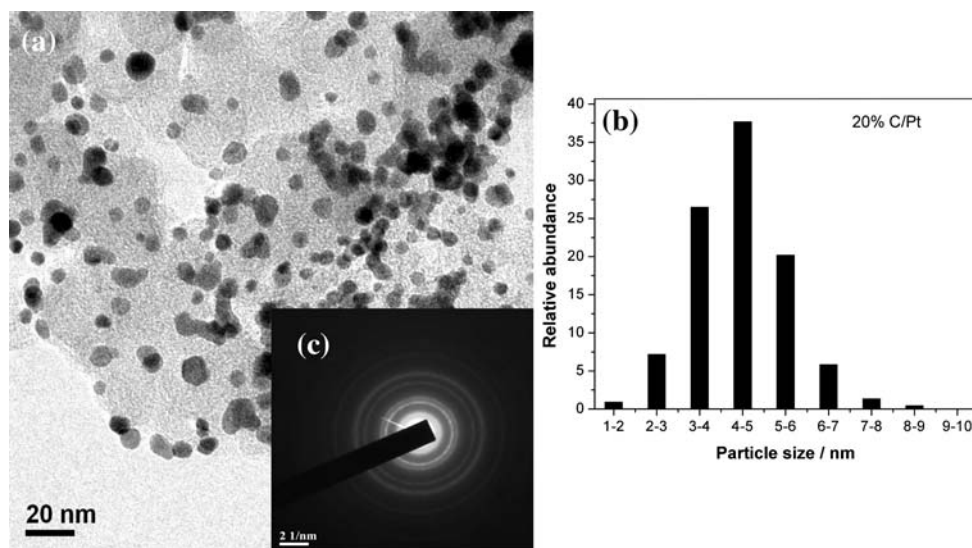


Fig. 3 **a** HRTEM image, **b** particle size distribution, and **c** selected area diffraction pattern (SADP) of C/Pt-a

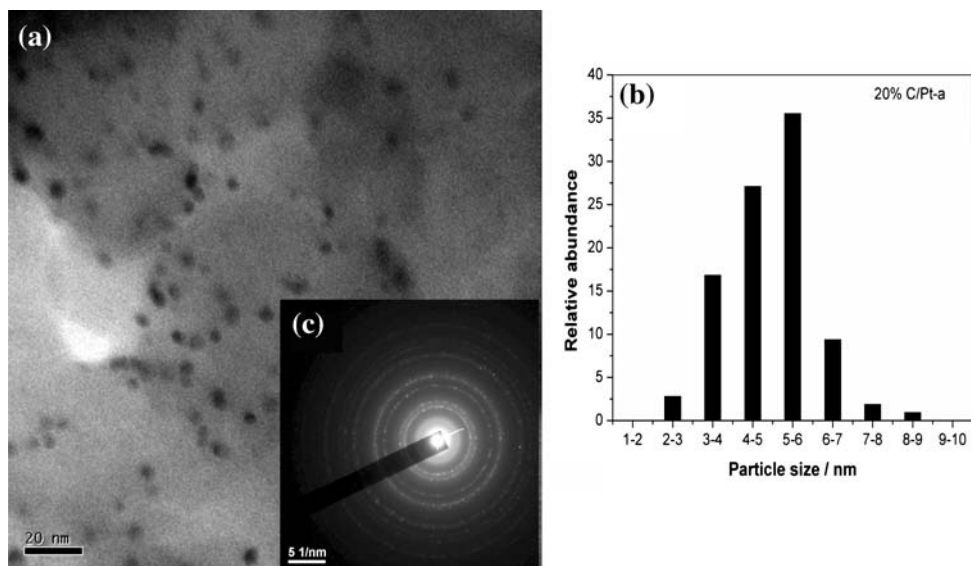


Fig. 4 **a** HRTEM image, **b** particle size distribution, and **c** selected area diffraction pattern (SADP) of C/Pt-b

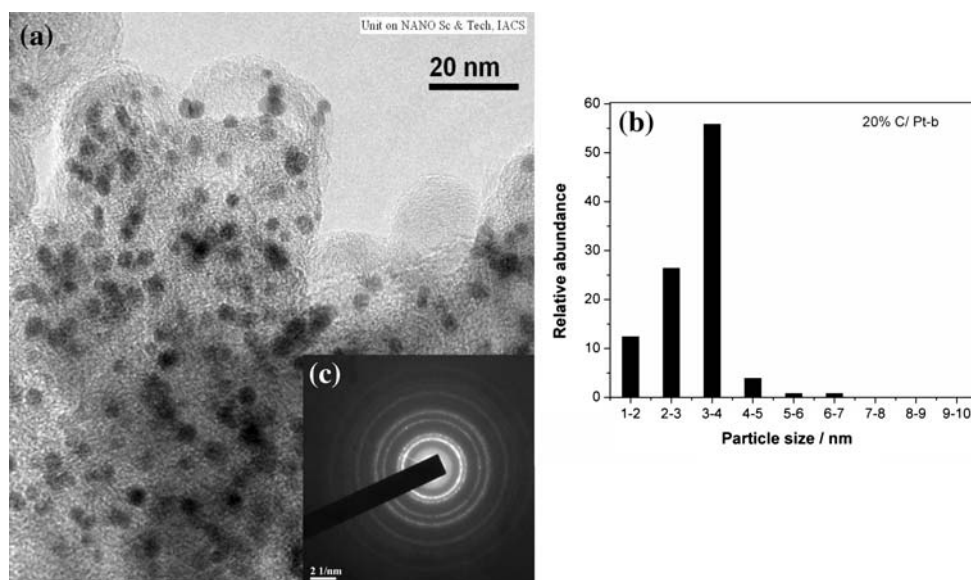
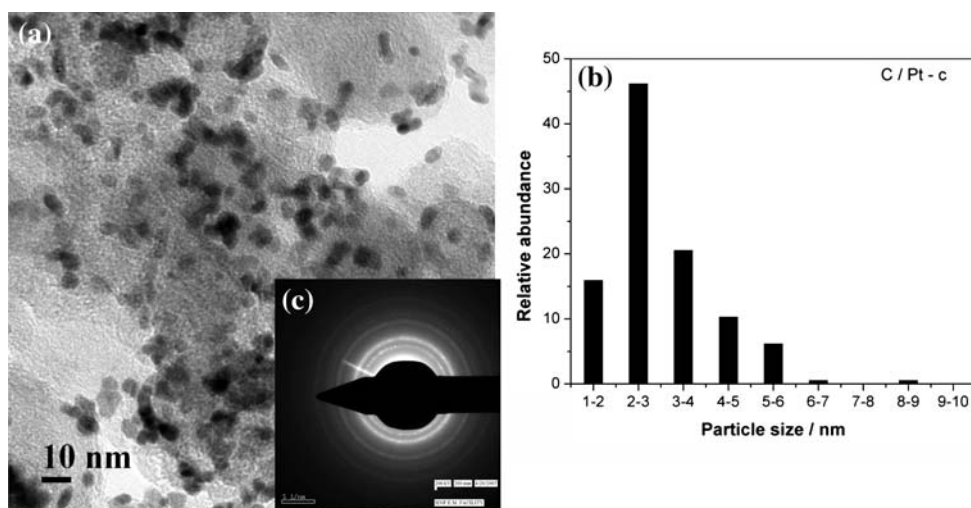


Fig. 5 **a** HRTEM image, **b** particle size distribution, and **c** selected area diffraction pattern (SADP) of C/Pt-c



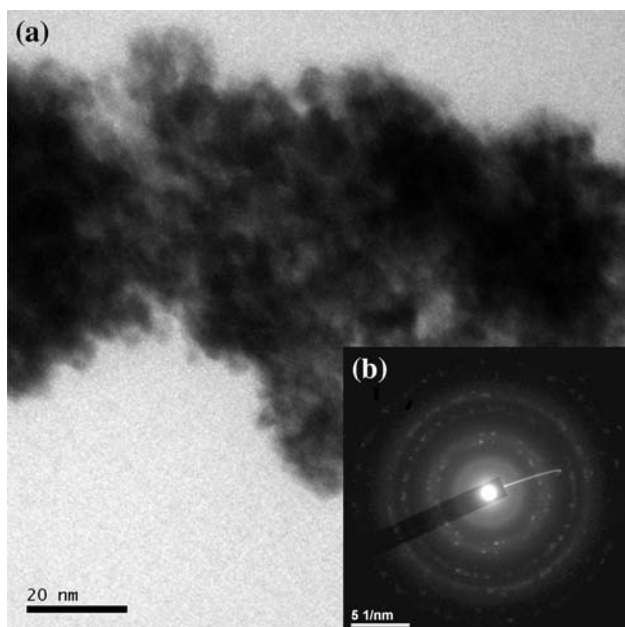


Fig. 6 **a** HRTEM image and **b** selected area diffraction pattern (SADP) of C/Pt-d

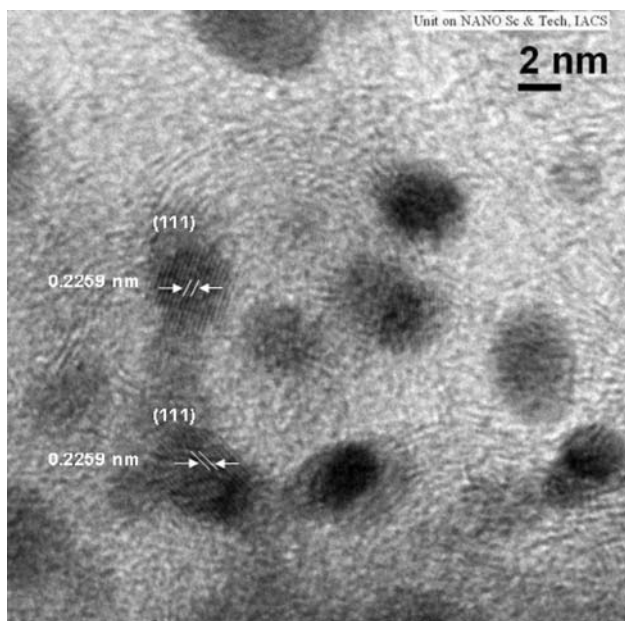


Fig. 7 Fringe pattern of C/Pt-c

equal. The volume weighted average sizes of the particles for all the catalysts calculated from the XRD peak widths agreed well with the TEM results.

In order to achieve precise value of the catalyst surface area and to get an overview of the textural properties of the Pt catalyst matrix, BET method was employed, for all the prepared catalysts. From Fig. 8, the Vulcan XC-72 carbon exhibits a typical reversible curve representative of type-IV/III nitrogen adsorption and desorption isotherm, while

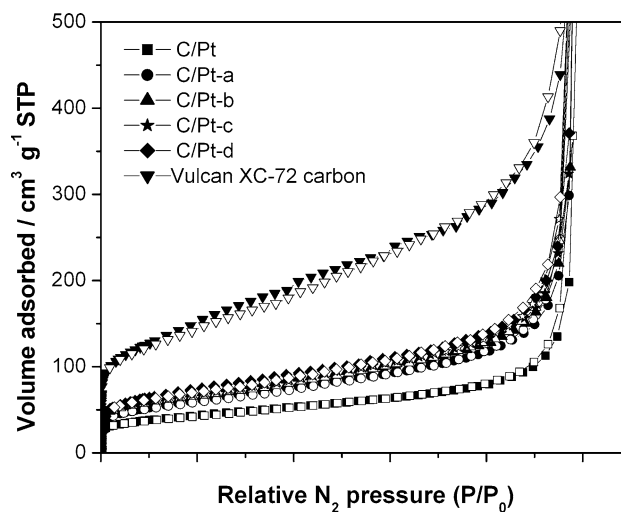
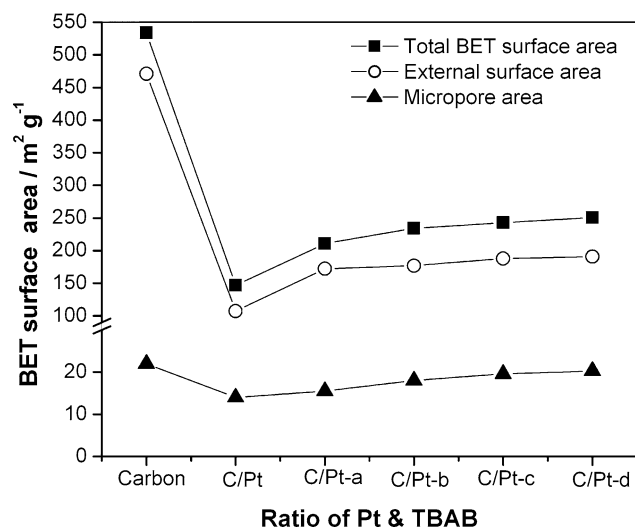


Fig. 8 Nitrogen adsorption (filled) and desorption (unfilled) isotherm for different catalysts

the different TBAB-stabilized Pt catalysts on such carbon support show a typical reversible curve representative of type-III pattern of the same according to the Brunauer–Deming–Deming–Teller (BDDT) classification. Both the type of hysteresis are attributed to cylindrical pores. The adsorption isotherm of the carbon support is associated with capillary condensation in predominantly mesoporous structure, while the structure of different TBAB-stabilized C/Pt catalysts is a combination of micropores and mesopores. The steep rise in the adsorption of N₂ at higher relative pressure (P/P_0) of carbon and all the TBAB-stabilized catalysts reflected the presence of mesopores in carbon. The surface area was found to decrease with the introduction of metal Pt on the carbon support, indicating impregnation or anchoring of metal particles inside mesopores of the carbon [29]. The different textural properties are summarized in Table 2. Figure 9 shows the evolution of BET surface areas of carbon and the different catalysts. A sharp fall is observed in the BET areas of all the TBAB-stabilized C/Pt catalysts as compared to the Vulcan XC-72 carbon; however, rise in TBAB level increases the total BET surface area along with the external surface area, while the micropore area of the catalyst surface remained almost the same. This indicates that the TBAB-stabilized Pt particles not only intercalate into the micropore of the graphite support but also grow on the external surface area of the support. The total BET area is therefore compromised with these two effects, since large quantity of micropores can enhance the absorbability of the catalyst and extend the active sites, and there is a possibility of better utilization of Pt particles during electro catalysis. Thus, stabilizing agent has a direct influence on metal dispersion and metal–support interaction. BJH model calculations of

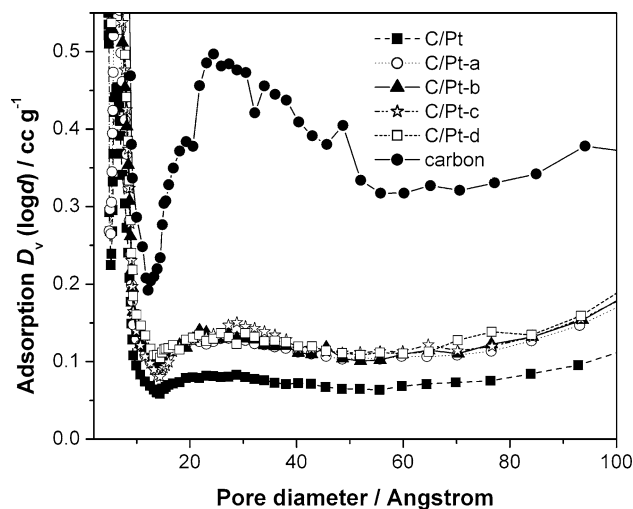
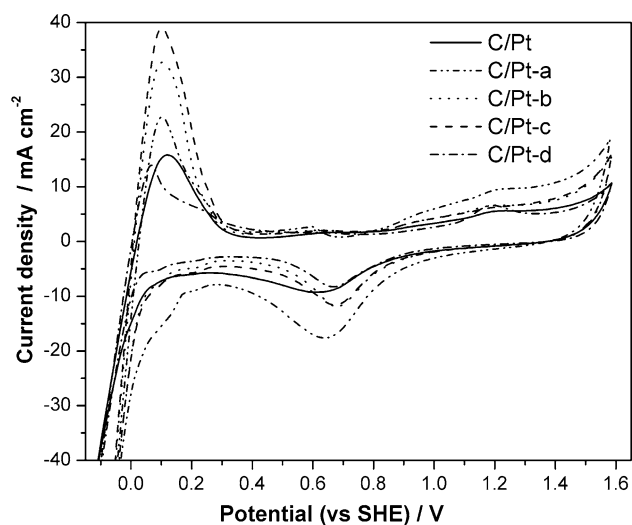
Table 2 Textural properties of various 20% C/Pt and TBAB-stabilized Pt catalysts

	Only carbon	C/Pt	C/Pt-a	C/Pt-b	C/Pt-c	C/Pt-d
BET surface area, S_{BET} ($\text{m}^2 \text{g}^{-1}$)	534.0	146.9	210.8	234.2	242.9	250.8
t-plot micropore area, S_{m} ($\text{m}^2 \text{g}^{-1}$)	22.0	14.0	15.5	18.0	19.6	20.3
t-plot external surface area, S_{Ex} ($\text{m}^2 \text{g}^{-1}$)	471.2	107.3	172.2	176.9	187.9	190.8
t-plot micropore volume, V_{m} (cc g^{-1})	0.0327	0.0205	0.0215	0.0296	0.0314	0.0321
Pore volume, V_{t} (cc g^{-1})	1.619	0.8991	1.488	1.540	1.614	2.033
Adsorption average pore width (nm)	121.3	245.1	252.2	263.0	265.8	323.4

**Fig. 9** Comparison of different surface areas of C/Pt and different TBAB-stabilized C/Pt catalysts

pore volume and pore size distributions were performed for the adsorption branch of the isotherm and the results are shown in Table 2. Although pore size of Vulcan XC-72 carbon remains exclusively in the mesoporous range those for the TBAB-stabilized C/Pt catalysts are found to cover both the mesopore and the micropore range which is presented in the pore size distribution curve (Fig. 10). The pore size and volume increase steadily with the higher extent of TBAB in the preparative bath. However, the BET parameter for C/Pt-d is not in conjunction with its electrocatalytic function as described in the following section. Here two possibilities may be considered: (i) the extensive finer grains of Pt in C/Pt-d may not form favorable sites of adsorption of the organic molecules (ii) even if the reaction proceeds the intermediates formed get entrapped into the highly porous matrix of C/Pt-d, making the oxidation kinetics more sluggish when compared to the others. Thus, the textural properties of the catalyst surface play a significant role in distributing the favorable sites for the dissociative adsorption of the organic molecules in course of the oxidation reaction.

Figure 11 shows the voltammograms of the protected and nonprotected C/Pt nanocatalysts in 0.5-M H_2SO_4

**Fig. 10** Pore size distributions calculated from nitrogen adsorption-desorption isotherm for different catalysts**Fig. 11** Voltammograms recorded of 20% C/Pt and TBAB-stabilized C/Pt catalysts in nitrogen-purged 0.5-M H_2SO_4 at a scan rate of 50 mV s^{-1}

solution. The C/Pt-c catalyst exhibits an enhanced catalytic feature in the voltammogram. The higher current in the hydrogen region (from -0.02 to -0.18 V vs SHE) is an

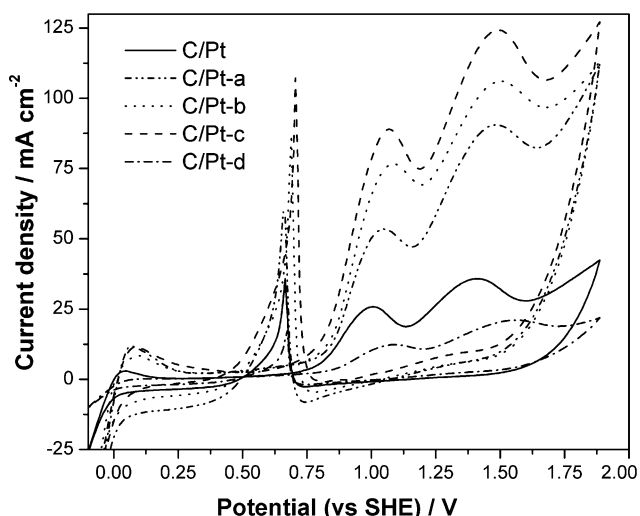


Fig. 12 Cyclic voltammograms of ethanol electrooxidation on C/Pt and TBAB-stabilized C/Pt catalysts. Electrolyte is nitrogen-purged 0.5-M H₂SO₄ solution containing 1.0-M ethanol. The scan rate was 50 mV s⁻¹

indication of pronounced activation of the surface through the narrowly distributed Pt nanoparticles that raises the hydrogen desorption current so high.

Figure 12 shows the CVs for all the catalysts in solution containing 0.5-M H₂SO₄ and 1-M CH₃CH₂OH. The ethanol oxidation current is found to be the highest and the lowest for the C/Pt-c and C/Pt-d catalysts, respectively. Further, the early commencement of oxidation process within the potential range 0.78–0.98 V versus SHE demonstrates higher electrochemical activity of the C/Pt-c catalyst when compared to the others. To substantiate the above view, cyclic voltammograms (Fig. 13) were also

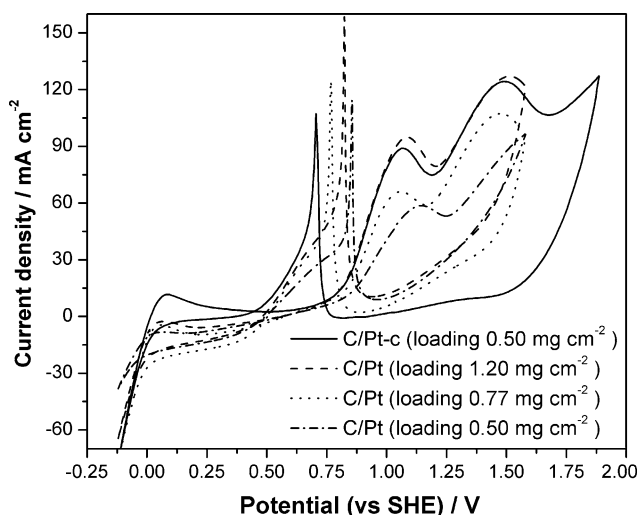


Fig. 13 Comparisons of ethanol electrooxidation on 20% C/Pt catalysts with different loadings and a TBAB-stabilized C/Pt catalyst (C/Pt-c) at room temperature. Scan rate: 50 mV s⁻¹

recorded for Pt catalyst prepared at higher loadings of 0.77 and 1.2 mg cm⁻² in absence of TBAB. Interestingly, the ethanol oxidation current produced by TBAB-stabilized electrode, C/Pt-c with a loading of 0.5 mg cm⁻², was found to be at par with the nonprotected catalyst bearing a loading of 1.2 mg cm⁻² and significantly higher than that obtained with 0.77 mg cm⁻² loading of C/Pt. Thus, it appears that TBAB-stabilized Pt matrix in spite of having lower loading, utilizes the maximum electrochemically active surface area. This becomes one of the desirable features associated with the use of stabilizing agent which besides rendering optimum size distribution and controlled dispersion of the metal particles throughout the catalyst surface is also capable of projecting the active planes of the nano-crystallites as favorable sites for the electrooxidation reaction. This in fact complies with the challenge of high utilization of precious metals at minimum possible loading during the fuel cell reaction.

Figure 14 shows the current–potential behavior during steady state polarization studies of ethanol electrooxidation on the prepared electrodes. At a potential of 1.18 V versus SHE, there is a 3-fold increase in electrooxidation current density on varying the TBAB content from 0 to 50% of catalyst in the chemical bath. This significant increase in current density implies that stabilization of the catalyst particles is of utmost importance in promoting active sites for electrooxidation reaction.

In order to ascertain the long-term stability of the electrodes, chronoamperograms were also recorded at 0.58 V versus SHE for 1 h as shown in Fig. 15. In all the chronoamperometric curves, there is a sharp initial current drop followed by a slower decay. Taking into account that ethanol molecules are favorably adsorbed on a required

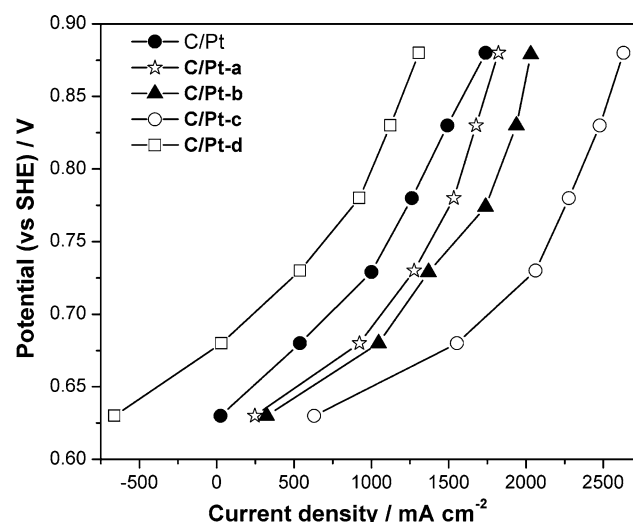


Fig. 14 Steady state polarization plots in 1.0 M EtOH + 0.5 M H₂SO₄ of different catalysts

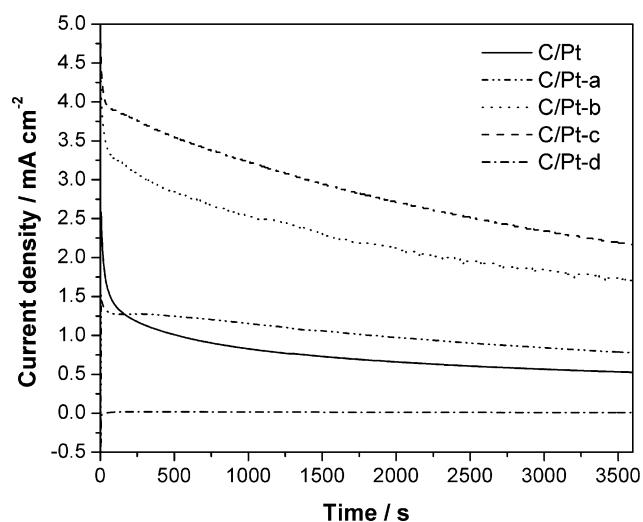


Fig. 15 Chronoamperograms recorded for 1 h at the potential of -0.1 V (MSE) in nitrogen-purged 1.0 M EtOH + 0.5 M H_2SO_4 of C/Pt and different TBAB-stabilized catalysts

ensemble of Pt surface atoms and that adsorption is suppressed on agglomerated Pt particles, it follows that the stabilizing agents not only decrease the particle size and reduce aggregation with increase of Pt-TBAB ratio in the preparative bath but also ensure facile reaction kinetics at the extensive reaction sites. The chronoamperometric experiments reveal that C/Pt-c catalyst offers the most stable and electrochemically active catalyst matrix for ethanol oxidation.

Nyquist plots obtained for ethanol oxidation on the carbon-supported Pt and TBAB-stabilized Pt electrodes in 0.5 -M H_2SO_4 at 0.58 V versus SHE are presented in Fig. 16 which shows the trend of R_{ct} in the descending order of C/Pt-c < C/Pt-b < C/Pt-a < C/Pt < C/Pt-d. The significant decrease in the magnitude of R_{ct} with increasing level of TBAB from C/Pt-a to C/Pt-c indicates an enhancement in the charge transfer kinetics, whereas C/Pt-d catalyst with highly raised R_{ct} values appears to be deactivating the charge transfer kinetics of ethanol oxidation. The results closely resemble the features of voltammograms and polarization studies presented in the preceding sections. Thus, the optimum use of stabilizing agent offering high electrochemically active area probably renders the oxidation reaction more facile.

Stabilizing effect of TBAB

Stabilization of the Pt particles by TBAB can be discussed mainly from the viewpoint of electrostatic effect and steric hindrance because of the cationic nature and hydrophobic organic moieties of the stabilizing agent (TBAB) as shown in Fig. 17

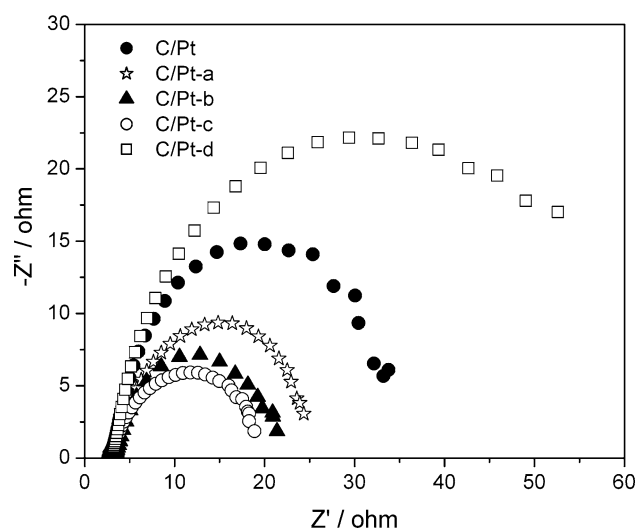
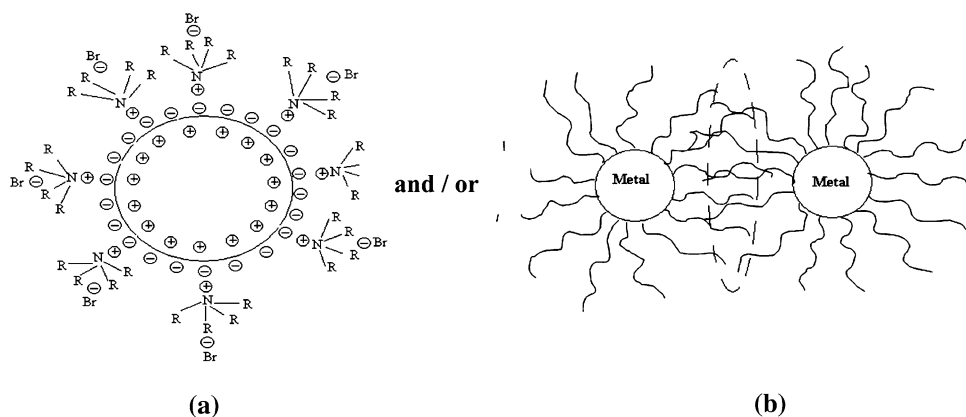


Fig. 16 Nyquist plots of ethanol oxidation on C/Pt and TBAB-stabilized C/Pt catalysts at -0.1 V electrode potential

Usually Pt metals are formed in aqueous medium through hydrosol. The protection of Pt sols from merging into larger particles is provided by the electrostatic attraction of the oppositely charged ammonium ion of TBAB, keeping one particle apart from the other. On the other hand, steric stabilization is provided by shielding the metal core with organic chain molecules. The tetraalkylammonium ions (NR_4^+) surrounding the negatively charged metal core of the particles inhibit the particles from undergoing any kind of agglomeration [25]. The coverage of the metal particles by the large lipophilic alkyl groups exerts a remarkable stability to the particles. It is worthwhile to mention the study of Bonnemann et al. [20] who made an extensive investigation on the stabilization mechanism in their synthesis of homogeneous catalyst using the surfactant tetraoctylammonium bromide (TOAB) combined with the reducing agent $K[BEt_3H]$ in THF. In the present investigation, a different preparative approach has been adopted with a lower homologue of TOAB, i.e., TBAB, which is coupled with the metal salt prior to the reduction step. Among the catalyst under consideration, the stabilization effect is most pronounced in the C/Pt-c, as reflected in the uniform and narrow size distribution of finer Pt particles on the carbon support. This is probably because a strong coordination affinity of the stabilizing agent with $PtCl_6^{2-}$ ions could be attained at higher molar concentration of TBAB in the bath, and thereby controls the reduction of $PtCl_6^{2-}$ ions which assist in the nucleation over the surface. The XRD and TEM results show that the TBAB not only plays significant role as a stabilizing agent but also the different concentrations of TBAB exert some fruitful influence in controlling the growth of the Pt

Fig. 17 **a** Electrostatic charges and **b** steric charges

particles and their dispersion over the carbon support. Although the preceding XRD section has predicted large electro active surface area for C/Pt-d, compared to the others, but there is no such electrochemical activity shown by C/Pt-d, as it would be. In this catalyst formulation, the excessive porosity of the bulk of the material (support and catalyst) has prevented the formation of ensembles of active Pt sites required for ethanol adsorption. Use of stabilizing agent in moderate concentration can therefore curb the growth of particles and achieve narrow distribution to the desired extent, enabling the projection of the active crystal planes as well as revealing its highest electrochemical activity. Among all, the C/Pt-c catalyst is expected to be the optimum in offering its active sites.

Conclusion

The investigations have shown that the borohydride reduction of Pt metal precursors can be made very effective by the optimal use of stabilizing agent, TBAB, in producing well-dispersed Pt metal nano-particles for use in fuel cell reactions. The TBAB acts as the stabilizing agent and stabilizes the nanoparticles without interfering with the deposition process. Moreover, controlled use of TBAB not only leads to the desired size distribution but also becomes effective in exposing the active crystallite planes for triggering the oxidation process. It is interesting to note that TBAB modifications in the synthetic route can execute the utilization of the catalyst particle to a great extent. Almost half of the loading of precious Pt is only required in the modified catalyst to maintain the same level of reactivity when compared with the nonprotected catalyst. The optimum requirement of TBAB is 50% with respect to the Pt precursor in the chemical bath during loading of the carbon support by Pt particles for fabrication of the catalyst matrix used for fuel cell reactions.

Acknowledgements Financial support from the Department of Science and Technology (DST), New Delhi is gratefully

acknowledged. The authors would also like to appreciate Ministry of Human Resource and development (MHRD), Govt. of India for their technical support on BET measurement.

References

- Zhou WJ, Zhou B, Li WZ, Zhou ZH, Song SQ, Sun GQ, Xin Q, Douvartzides S, Goula M, Tsiakaras P (2004) *J Power Sour* 126:16
- Liu Z, Shamsuzzoha M, Ada ET, Reichert WM, Nikles DE (2007) *J Power Sour* 164:472
- Du HY, Wang CH, Hsu HC, Chang ST, Chen US, Yen SC, Chen LC, Shih HC, Chen KH (2008) *Diam Relat Mater* 17:535
- Park S, Xie Y, Weaver MJ (2002) *Langmuir* 18:5792
- Nores Pondal FJ, Vilella IMJ, Troiani H, Granada de Migue MSR, Scelza OA, Corti HR (2009) *Int J of Hydrogen Energy*. doi: [10.1016/j.ijhydene.2009.07.073](https://doi.org/10.1016/j.ijhydene.2009.07.073) (in press)
- Narayanan R, El-Sayed MA (2004) *Nano Lett* 4:1343
- Arenz M, Mayrhofer KJJ, Stamenkovic V, Blizanac BB, Tomoyuki T, Ross PN, Markovic NM (2005) *J Am Chem Soc* 127:6819
- Rajalakshmi N, Dhathathreyan KS (2008) *Int J Hydrogen Energy* 33:5672
- Thompson SD, Jordan LR, Forsyth M (2001) *Electrochim Acta* 46:1657
- Cherstiouk OV, Simonov PA, Savinova ER (2003) *Electrochim Acta* 48:3851
- Zhang X, Chan KY (2003) *Chem Mater* 15:451
- Liu Z, Lee J, Han M, Chen W, Gan L (2002) *J Mater Chem* 12:2453
- Watanabe M, Uchida M, Motoo S (1987) *J Electroanal Chem* 229:395
- Prabhuram J, Manoharan R (1998) *J Power Sour* 74:54
- Castro Luna AM, Camara GA, Paganin VA, Ticinelli EA, Gonzalez ER (2000) *Electrochem Commun* 2:222
- Goodenough JB, Hamnett A, Kennedy BJ, Manoharan R, Weeks SA (1990) *Electrochim Acta* 35:199
- Roth C, Martz N, Fuess H (2001) *Phys Chem Chem Phys* 3:315
- Lizcano-Vulbuena WH, Paganin VA, Leite CA, Galembeck F, Gonzalez ER (2003) *Electrochim Acta* 48:3869
- Guo JW, Zhao TS, Prabhuram J, Wong CW (2005) *Electrochim Acta* 50:1973
- Bonnmann H, Brijoux W, Brinkmann R, Dinjus E, Fretzen R, Jousset T, Koppler B, Korall B, Neiteler P, Richter J (1994) *J Mol Catal* 86:129
- Bonnemann H, Braun G, Brijoux W, Brinkmann R, Tilling S, Seevogel K, Siepen K (1996) *J Organomet Chem* 520:143

22. Wang X, Hsing IM (2002) *Electrochim Acta* 47:2981
23. Schmidt TJ, Noeske M, Gasteiger A-H, Behm RJ, Britz P, Brijoux W, Bonnemann H (1998) *J Electrochem Soc* 145(3):925
24. Paulus UA, Endruschat U, Feldmeyer GJ, Schmidt TJ, Bonnemann H, Behm RJ (2000) *J Catal* 195:383
25. Prabhuram J, Wang X, Hui CL, Hsing IM (2003) *J Phys Chem B* 107:11057
26. Kim T, Takahashi M, Nagai M, Kobayashi K (2004) *Electrochim Acta* 50:817
27. Chan KY, Ding J, Ren J, Cheng S, Tsang KY (2004) *J Mater Chem* 14:505
28. Yano H, Kataoka M, Yamashita H, Uchida H, Watanabe M (2007) *Langmuir* 23:6438
29. Samant PV, Rangel CM, Romero MH, Fernandes JB, Figueiredo JL (2005) *J Power Sour* 151:79